Schweizerischer Erdbebendienst
Service Sismologique Suisse
Servizio Sismico Svizzero
Swiss Seismological Service

ETH zürich

# SITE CHARACTERIZATION REPORT

# SAYF2: Ayent-Fortunau (VS) - Trafohaus

Manuel Hobiger, Paolo Bergamo, Francesco Panzera, Donat Fäh

Last Modification: 03/11/2020

Schweizerischer Erdbebendienst (SED)
Service Sismologique Suisse
Servizio Sismico Svizzero
Servizi da Terratrembels Svizzer

ETH Zürich
Sonneggstrasse 5
8092 Zürich
Schweiz
manuel.hobiger@sed.ethz.ch

# Contents

# Summary

The free-field strong-motion station SAYF2 was built close to the old station SAYF next to a transformer house in Ayent-Fortunau (VS). We performed a passive seismic array measurement and an active experiment to characterize the soil underneath the station. The measurements show a not very strong peak at around 2.15 Hz and additional peaks between 5 and 10 Hz for some array stations. The array measurements were analyzed with different techniques, namely 3-component high-resolution FK (HRFK), WaveDec and Spatial Autocorrelation (SPAC), with compatible dispersion curves. The active MASW Rayleigh wave dispersion curve complements the other curves at higher frequencies. The dispersion curves for the fundamental modes of Love and Rayleigh waves could be retrieved from around 7.7 to 39.5 Hz and 5.8 to 40.7 Hz, respectively, using the passive experiment. The active experiment yields a Rayleigh wave dispersion curve between 15.9 and 64.7 Hz.

The joint inversion of Love and Rayleigh wave dispersion curves and the Rayleigh wave ellipticity angle showed that the structure can be explained by models with interfaces at about 3.8 m, 18 m and 100 m depth, with the shear-wave velocity increasing from 230 m/s to over 1000 m/s. The $V_{S30}$ of the best models is about 476 m/s, corresponding to soil class B in EC8 and C in SIA261.

# 1 Introduction

In the framework of the second phase of the Swiss Strong Motion Network (SSMNet) renewal project, a new station was planned in Ayent-Fortunau (VS), to replace the old station SAYF, which was located in a transformer house.
The new station is a free-field station, located in a distance of about 7 m outside of the transformer house. It is called SAYF2 and went operational on 29 April 2015. The location of the station is shown in Fig. 1.

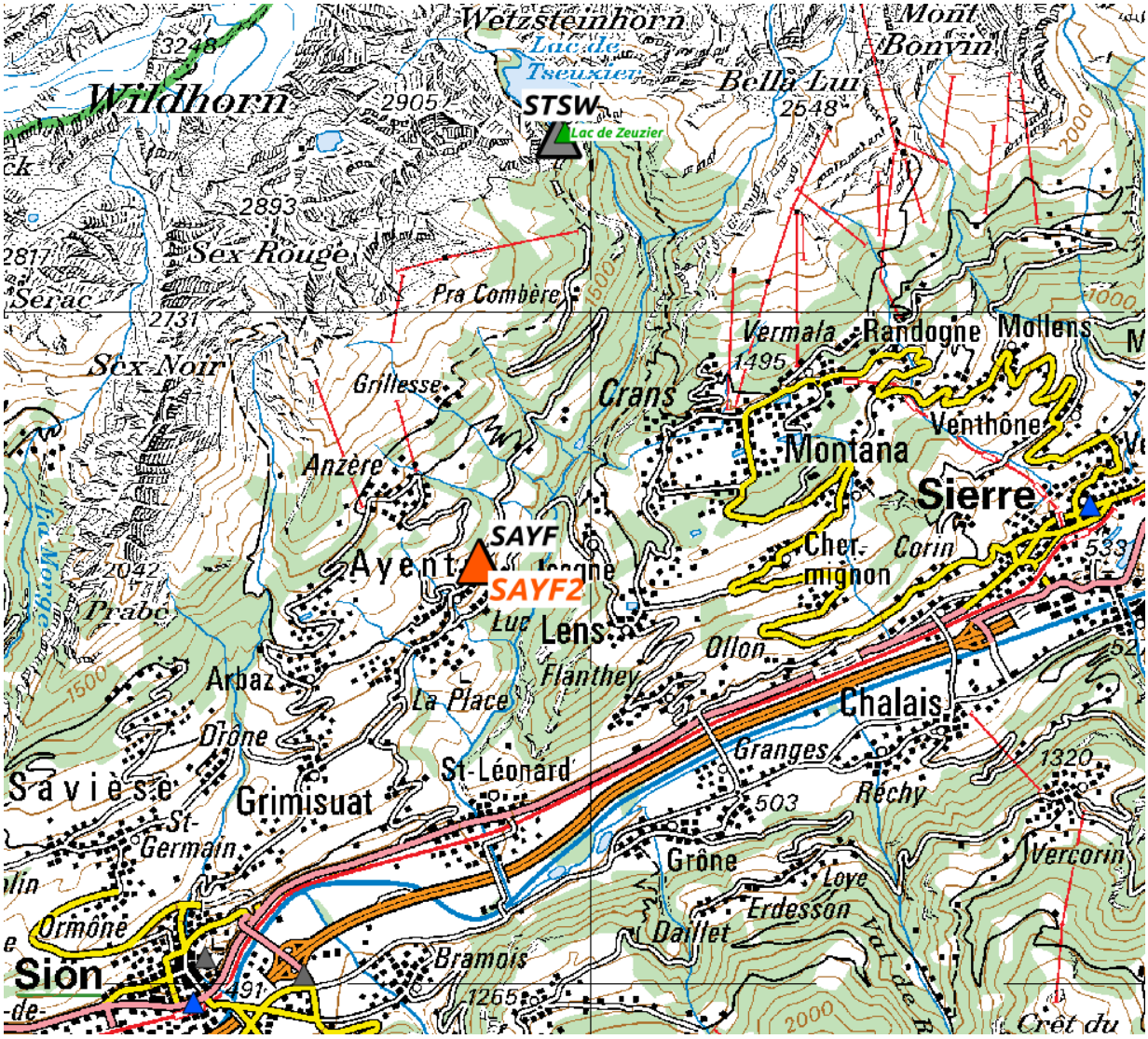


Figure 1: Map showing the location of station SAYF2 in Ayent-Fortunau. Other stations in the area are indicated as well. ©2020 swisstopo (JD100042)

# 2 Geological setting

A geological map of the surroundings of station SAYF2 is shown in Fig. 2. The station is located in a small bed of fine-grained scree. Further north, marl is found, and to the south, moraine deposits are predominant. Most stations of the passive array measurement were located on the scree, but some were located on moraine.

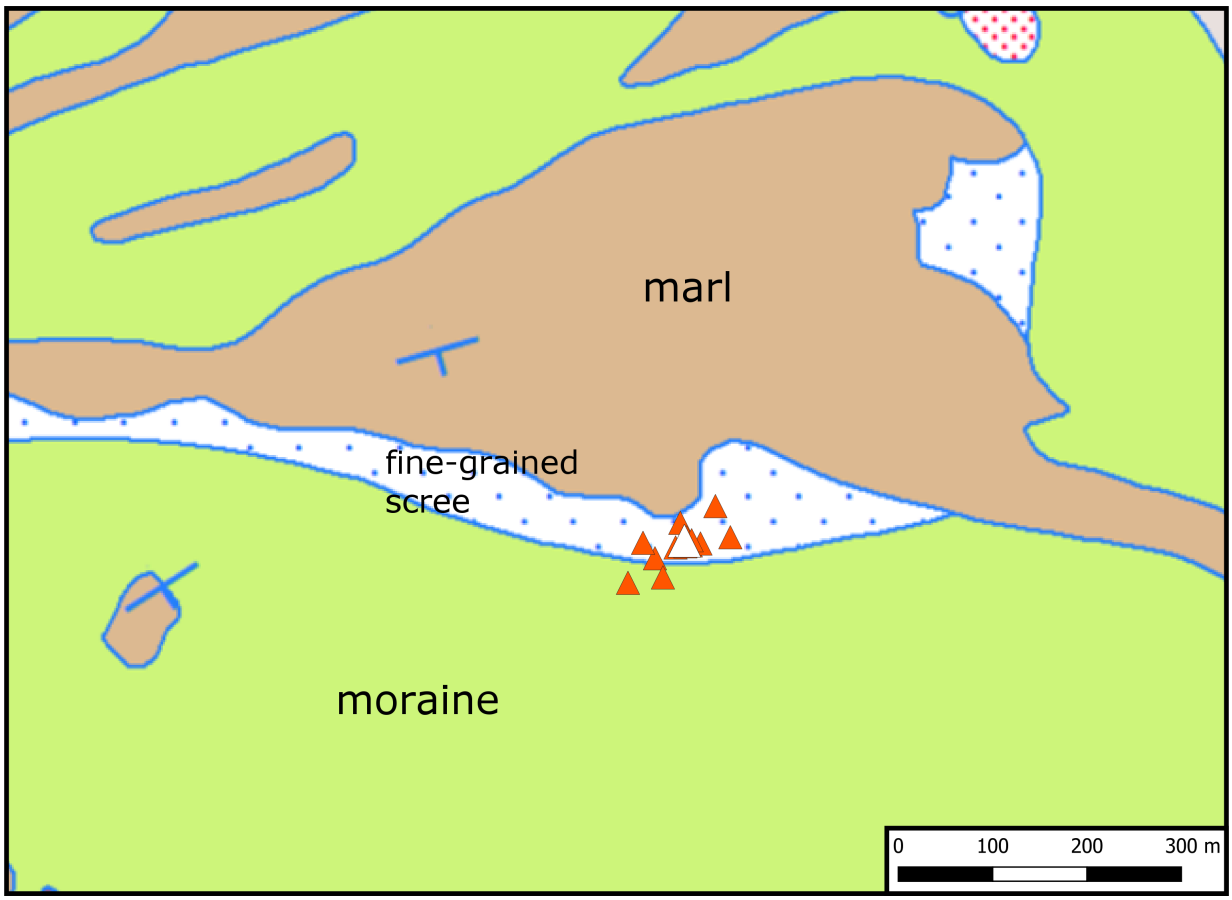


Figure 2: Geological map of the area around station SAYF2 (white triangle) with the different stations of the array measurement (orange triangles). According to the geological atlas, station SAYF2 and most stations of the passive array measurement lie on fine-grained scree, some stations to the south lie on moraine. ©2020 swisstopo (JD100042)

# 3 Site characterization measurements

## 3.1 Data set

In order to characterize the local underground structure around station SAYF2, a passive seismic array measurement was carried out on 1 July 2015. The layout of the seismic measurements is shown in Fig. 3.
A single passive array measurement was performed. The array consisted of 15 stations arranged in a central circle of five stations with a radius of about 5 m around a central station, with the other nine sensors located more irregularly in the surroundings. The minimum and maximum inter-station distances were 4.9 m and 123.2 m, respectively. The names of the stations of the array are composed of "SAYF2" followed by a two-digit number (01 to 04, 06 to 12, 22, 24, 28, 32). The seismic stations consisted of Lennartz 3C 5 s sensors connected to Quanterra digitizers. A total of 11 digitizers were used. Eleven sensors were connected to the A channels of the digitizers and another four sensors were connected to B channels. The total recording time was 80 minutes.
In addition to the passive measurement, an active measurement using 24 geophones was performed. The geophones were located with 1.0 m spacings along a line. Seismic signals were generated by hammering with a sledgehammer ten times at each of six different shot locations. The shot locations were 1.8 m, 5.0 m and 10.0 m to the west of the westernmost geophone of the line and 1.0 m, 5.0 m and 10.0 m to the east of the easternmost geophone.
The station locations have been measured by a differential GPS system (Leica Viva GS10) which was set up to measure with a precision better than 5 cm. This precision was achieved for all stations except SAYF01, were the precision was 7.9 cm.

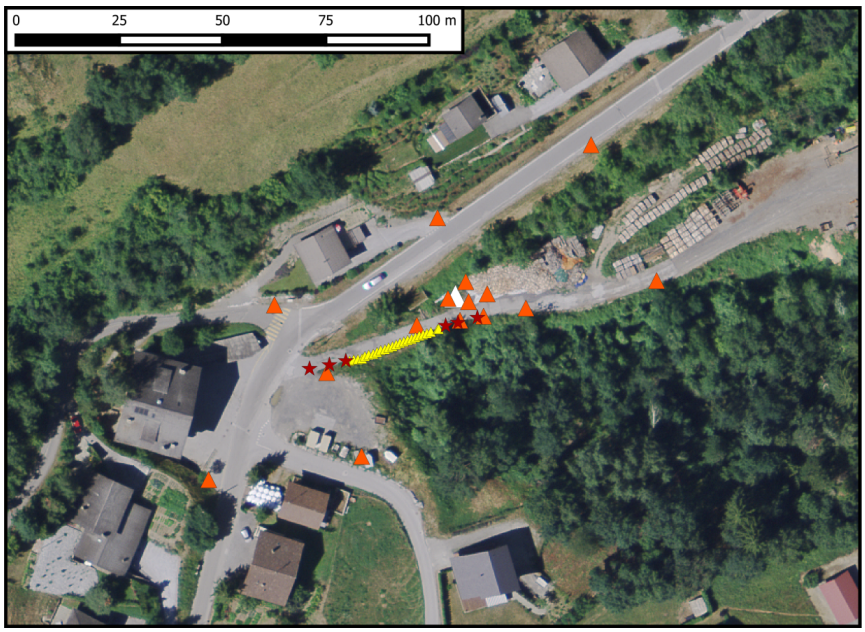


Figure 3: Layout of the array measurements around station SAYF2. The location of SAYF2 is indicated by the white triangle, the locations of the stations for the passive seismic measurement by the orange triangles. The yellow triangles indicate the geophone locations of the passive measurement. The red stars show the shot locations. 

## 3.2 H/V and RayDec ellipticity curves

Figure 4 shows the H/V curves determined with the time-frequency analysis method (Fäh et al., 2009) for all stations of the passive array. All curves are rather similar. They show two low-frequency peaks at around 0.3 and 0.7 Hz, which are not very pronounced. Another peak is found just above 2 Hz. At higher frequencies, the different curves have more variability and show another peak between 5.4 and 7.9 Hz.
The RayDec technique (Hobiger et al., 2009) is supposed to eliminate the contributions of other wave types than Rayleigh waves and give a better estimate of the ellipticity than the classical H/V technique. The RayDec ellipticity curves for all stations of the array measurement are shown in Fig. 4 and are similar to the H/V curves. However, the peak at 0.3 Hz is more pronounced. Station SAYF04, the closest station to the permanent station SAYF2, serves as a reference and will be used for the inversion. It shows a low peak at 2.15 Hz, but no very pronounced peak at higher frequencies.

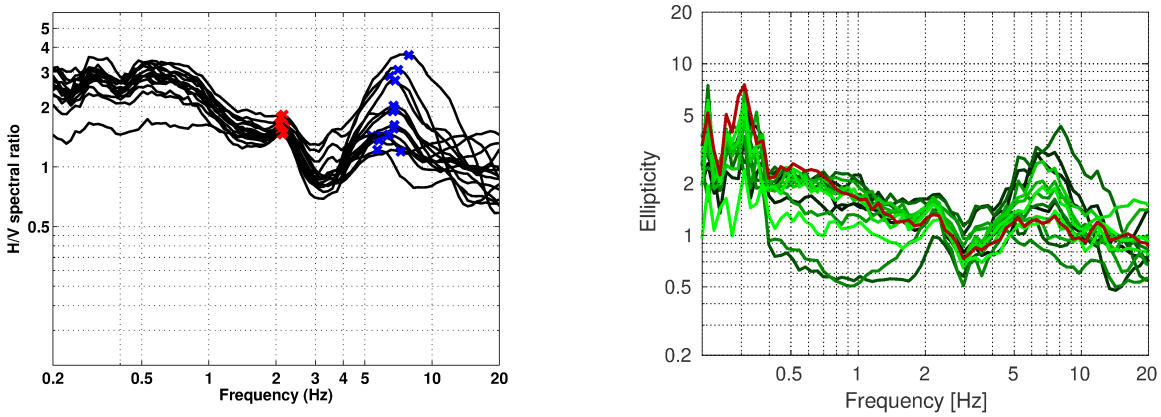


Figure 4: Left: Overview of the H/V measurements for the different stations of the array measurements. Right: RayDec ellipticities for all measurement stations. The red curve corresponds to SAYF04, the station closest to the permanent station SAYF2.

## 3.3 Polarization measurements

The polarization analysis was performed according to Burjánek et al. (2010) and Burjánek et al. (2012). The results for all stations of the array are similar. Only the results for SAYF040 are shown here.
There is no preferential linear particle polarization visible and we do not see indications for 2-dimensional polarization effects. At 6 Hz, there is a preferential strike direction along the topographic gradient. We interpret this frequency therefore as the eigenvibrations of the scree layer.

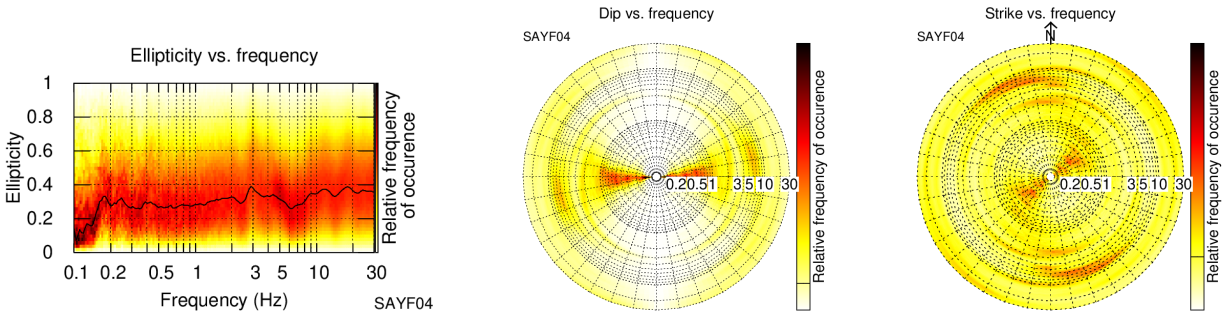


Figure 5: Polarization analysis of station SAYF04.

## 3.4 3-component high-resolution FK

The results of the 3-component high-resolution FK analysis (Poggi and Fäh, 2010) are shown in Fig. 6. On the transverse component, corresponding to Love waves, we can identify a dispersion curve between 7.7 and 38.4 Hz. However, the uncertainty is relatively large.
On the vertical component, corresponding to Rayleigh waves, we can identify one mode between 7.7 and 40.7 Hz, spanning the complete accessible frequency range. On the radial component, also related with Rayleigh waves, we can see the dispersion curve between 8.2 and 34.1 Hz.
The corresponding ellipticity curves of these modes are relatively flat.

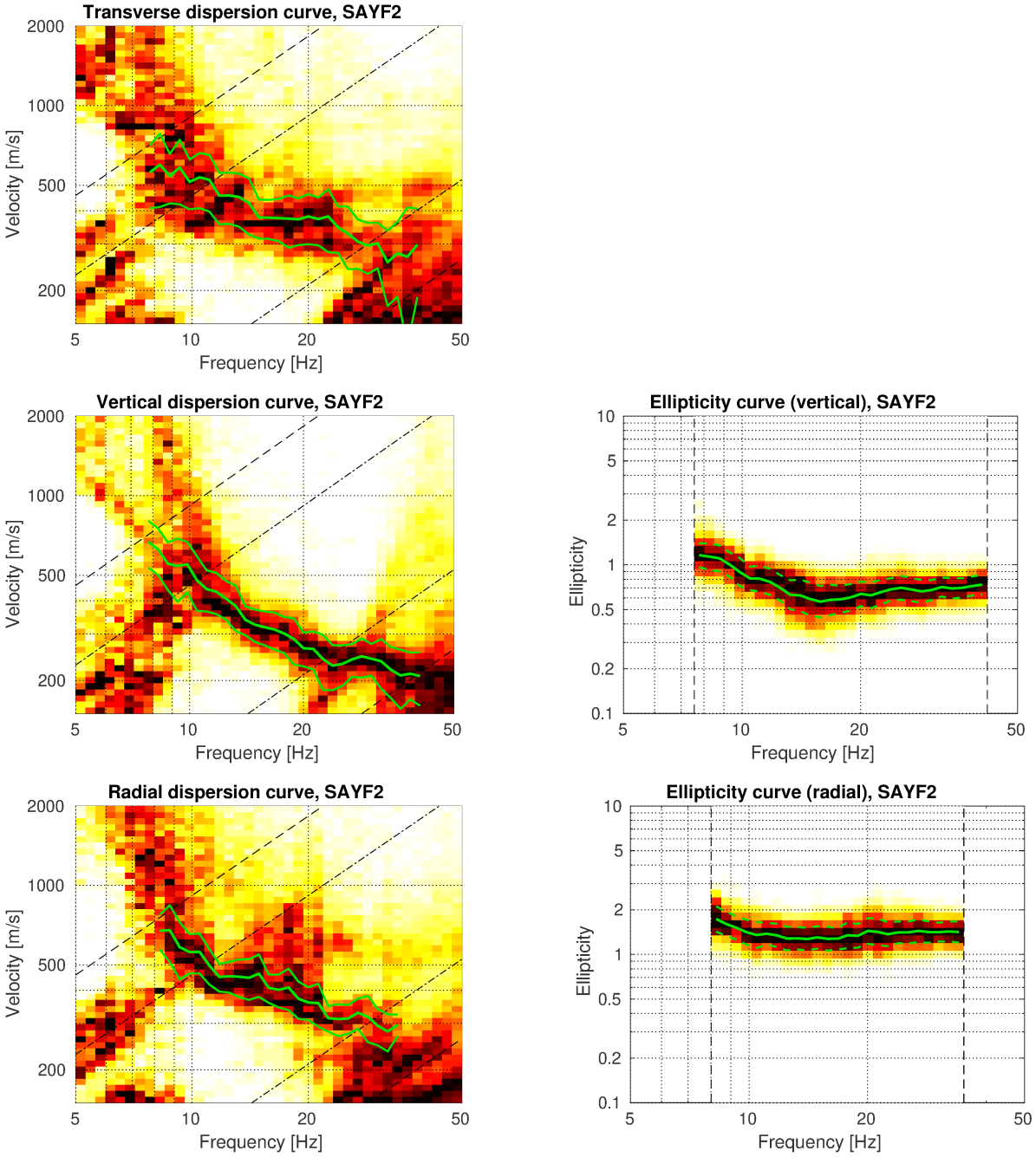


Figure 6: Dispersion and ellipticity curves obtained with the 3-component HRFK algorithm (Poggi and Fäh, 2010). In the left column, the dispersion curves for the transverse, vertical and radial components are shown, and in the right column the ellipticity curves corresponding to the dispersion curves picked on the vertical and radial components. The dashed and dotted black lines are the array resolution limits. The solid green lines are picked from the data, where the central line indicates the best values and the two outer lines the standard deviation.

## 3.5 WaveDec

The results of the WaveDec (Maranò et al., 2012) processing are shown in Fig. 7. This technique estimates the properties of single or multiple waves simultaneously with a maximum likelihood approach. In order to improve the results, the parameter $\gamma$, which modifies the sharpness of the wave property estimation, has been tuned. Here, a value of $\gamma = 0.2$ was used, corresponding to a predominantly maximum likelihood estimation. For Love waves, two dispersion curve branches are visible. The first one was picked between 7.7 and 16.4 Hz, the second one between 12.4 and 39.5 Hz.
For Rayleigh waves, a single dispersion curve is retrieved between 7.7 and 34.5 Hz. The ellipticity angle for the picked Rayleigh wave dispersion curve is negative over the whole frequency range.

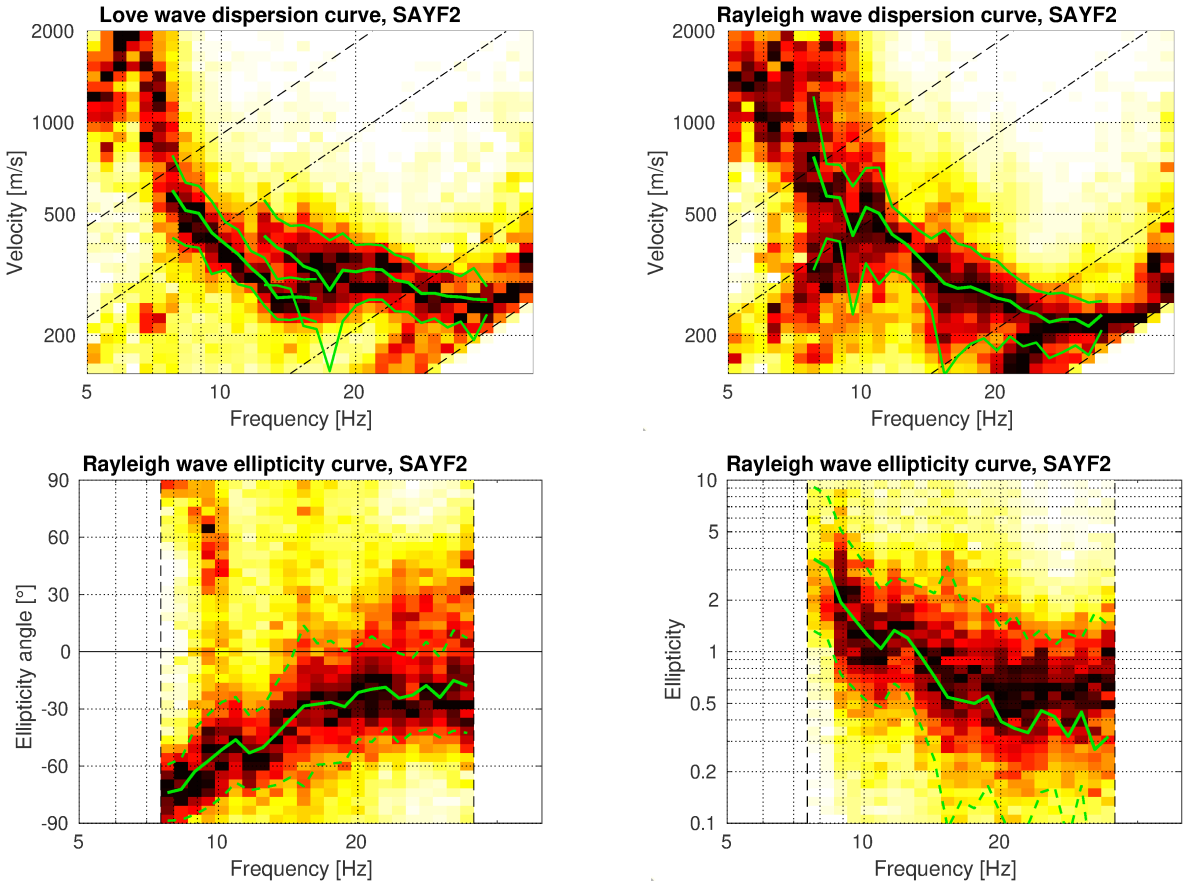


Figure 7: Top: Love (left) and Rayleigh (right) wave dispersion curves obtained with the WaveDec technique (Maranò et al., 2012). The dashed lines indicate the theoretical array resolution limits. Bottom: Rayleigh wave ellipticity angle curve for the picked dispersion curve (left) and Rayleigh wave ellipticity curve (right), i.e. the absolute value of the tangent of the ellipticity angle.

## 3.6 SPAC

The SPAC (Aki, 1957) curves of the vertical components have been calculated using the M-SPAC (Bettig et al., 2001) technique implemented in geopsy (Wathelet et al., 2005). Rings with different radius ranges had been defined previously and for all station pairs with distance inside this radius range, the cross-correlation was calculated over a wide frequency range. These cross-correlation curves are averaged for all station pairs of the respective ring and give the SPAC curves. The rings are defined in such a way that at least three station pairs contribute and their connecting vectors have a good directional coverage.
The SPAC curves for all defined rings are shown in Fig. 8. The black points indicate the data values which contributed to the final dispersion curve estimation, which was made with the function `spac2disp` of the geopsy package.
Using SPAC, we can retrieve a Rayleigh wave dispersion curve between 5.8 and 20.4 Hz.

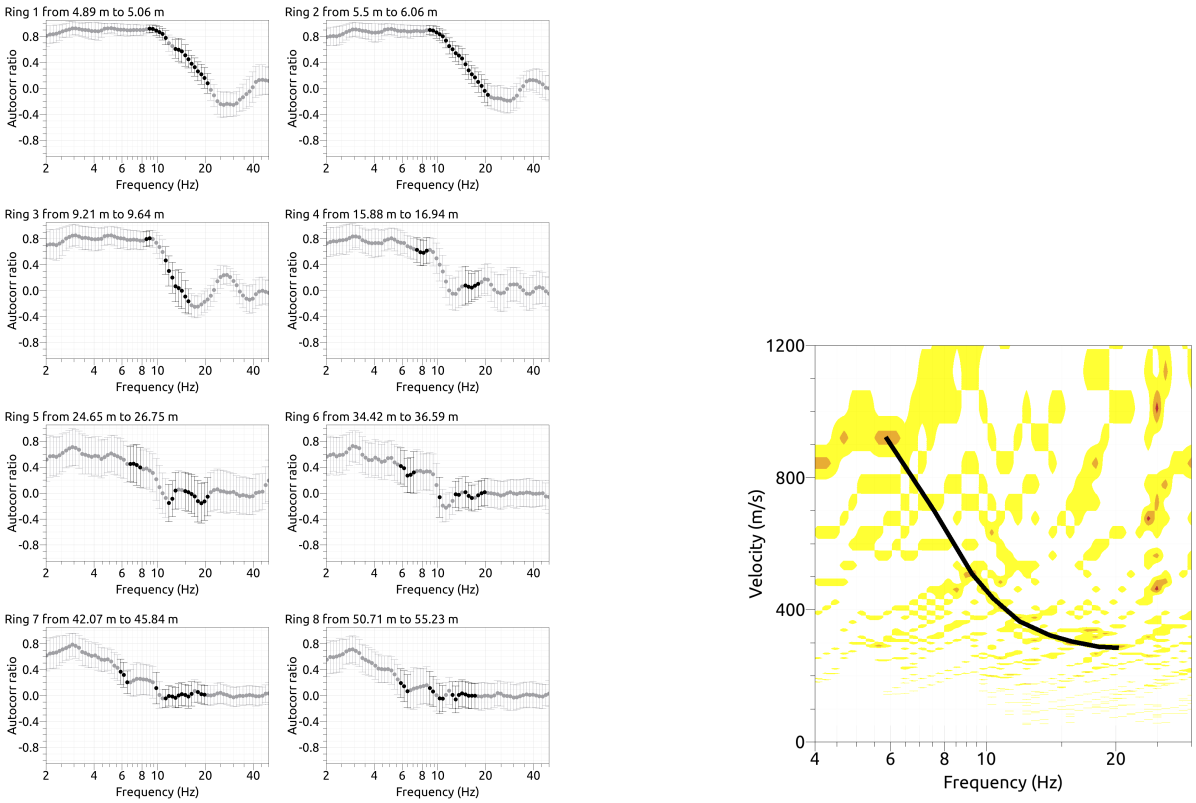


Figure 8: Left: SPAC curves for the different distance ranges. The black data points contributed to the dispersion curve estimation. Right: Resulting Rayleigh wave velocities. The black line corresponds to the picked dispersion curve.

## 3.7 Active measurement

The active hammering experiment was analyzed using the active FK technique implemented in geopsy (Wathelet et al., 2005). First, the signals of the different hammer shots at each shot point were stacked and analyzed, using only the vertical component signals. Then, the outputs of the six shot points where stacked (see Fig. 9) and a dispersion curve picked. The resulting curve ranges from 15.9 to 64.7 Hz.

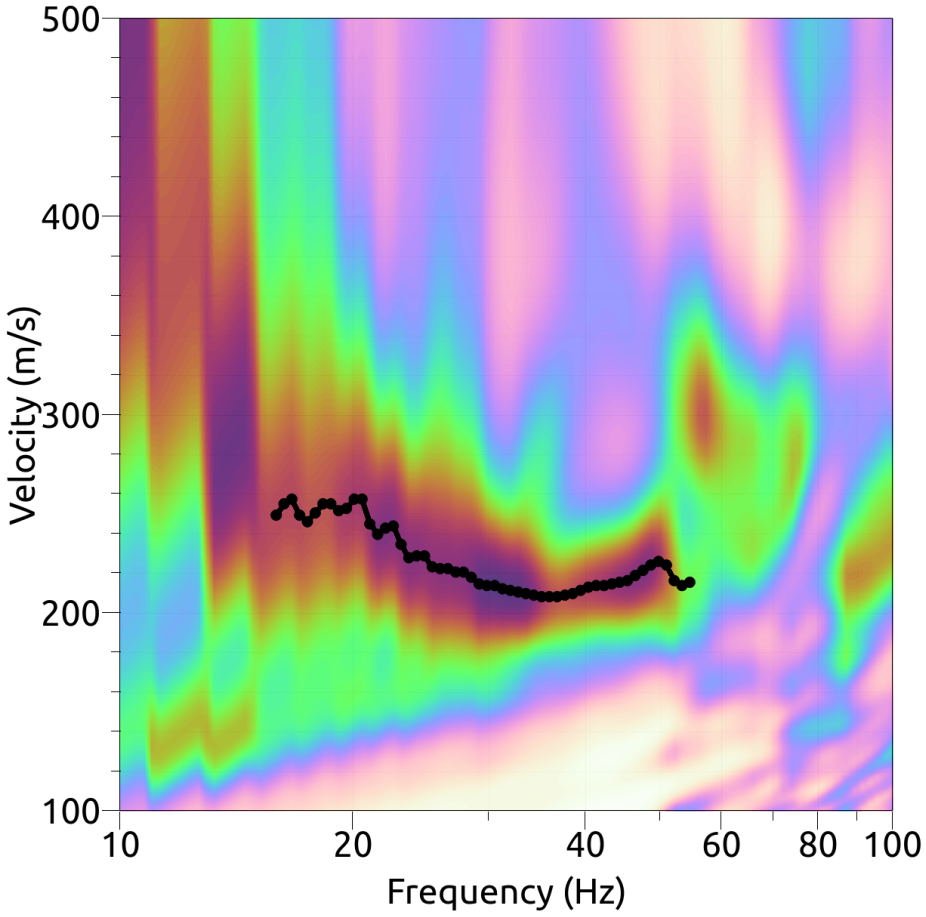


Figure 9: Result of the active measurement analysis of the vertical component of the geophones.

## 3.8 Summary

Fig. 10 gives an overview of the dispersion and ellipticity curves determined by the different methods.
For Love waves, HRFK gives a single continuous dispersion curve, while WaveDec finds two dispersion curves with unclear mode attribution. The second picked mode is actually in good agreement with the HRFK result, while the first WaveDec mode is slower than the HRFK results.
For Rayleigh waves, the different methods are in better agreement. The HRFK curve for the vertical component is in very good agreement with the WaveDec curve. Both fit also well with the SPAC curve, which actually reaches deeper frequencies. The radial HRFK curve is only in agreement with these curves below 12 Hz and deviates to higher velocities above and might correspond to a different mode there. The active curve corresponds well with the other curves and reaches higher frequencies.
The ellipticity curves retrieved using the different methods are in partial agreement. The vertical HRFK curve is in better agreement with the RayDec curve than the radial curve, supporting the hypothesis that the radial HRFK curve corresponds to a different mode. The WaveDec curve partially agrees with the RayDec curve. At 6 Hz, it shows a peak which is not visible in the RayDec curve for SAYF04. As other stations showed peaks around this frequency (Fig. 4), it might be that WaveDec as an array method is more influenced by those stations. In any case, the particle motion of the WaveDec curve is retrograde in the whole frequency range, indicating that there is no singularity in the ellipticity curve in the frequency range covered by WaveDec.

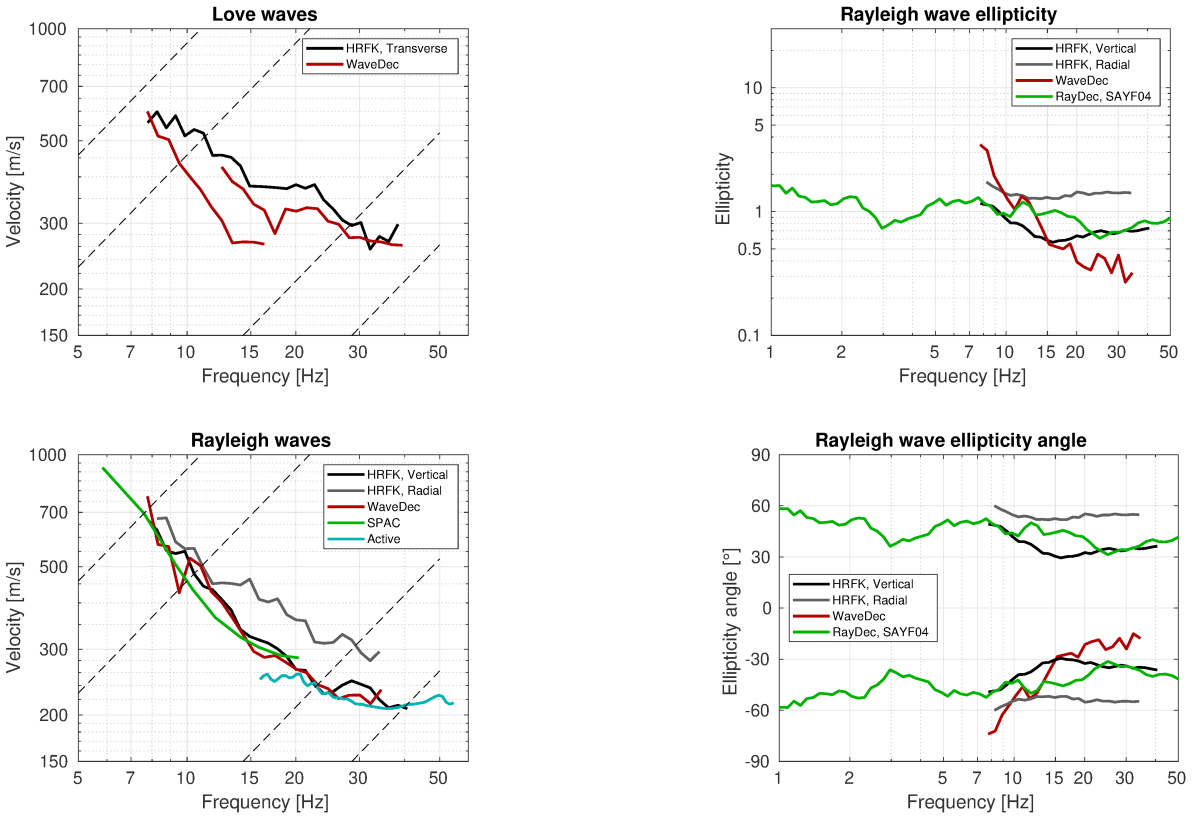


Figure 10: Overview of the Love and Rayleigh wave dispersion curves as well as the ellipticity and ellipticity angle curves for both arrays. The dashed lines indicate the theoretical resolution limits of the array. The RayDec ellipticity curve corresponds to station SAYF244.

# 4 Data inversion

## 4.1 Inversion targets

The curve picked for HRFK on the transverse component was assumed as the fundamental mode Love wave dispersion curve. For the Rayleigh wave dispersion curve, the picked HRFK curve for the vertical component was mainly used, adding some parts of the SPAC dispersion curve at low frequencies and of the active measurement curve at higher frequencies. As both the SPAC and the active curves were picked without error bars, reasonable uncertainties similar to the HRFK curve were assumed.
The RayDec curve was used as ellipticity angle information, assuming retrograde particle motion over the whole frequency range. The details of the inversion targets are indicated in Table 1 and the corresponding curves are shown in Fig. 11.

## 4.2 Inversion parameterization

Six different parameterizations have been used in total. The first five had free values of the depths and velocities of the different layers, ranging from four to eight layers (including the half-space). The last parameterization had fixed layer depths and consisted of 19 layers in total. The main interface depths resulting from the 8-layer inversion were used in the fixed-layer approach. The P-wave velocities were allowed to vary up to 5000 m/s. The S-wave velocities were allowed to range from 30 to 3500 m/s. The deepest layers were parameterized to reach a depth of 150 m maximum. The density was fixed to 2 300 $kg/m^3$ for the lowest layer, to 1 900 $kg/m^3$ for the superficial layer (or the first three layers in the fixed-layer case) and to 2 100 $kg/m^3$ for all other layers. No low-velocity zones were allowed.

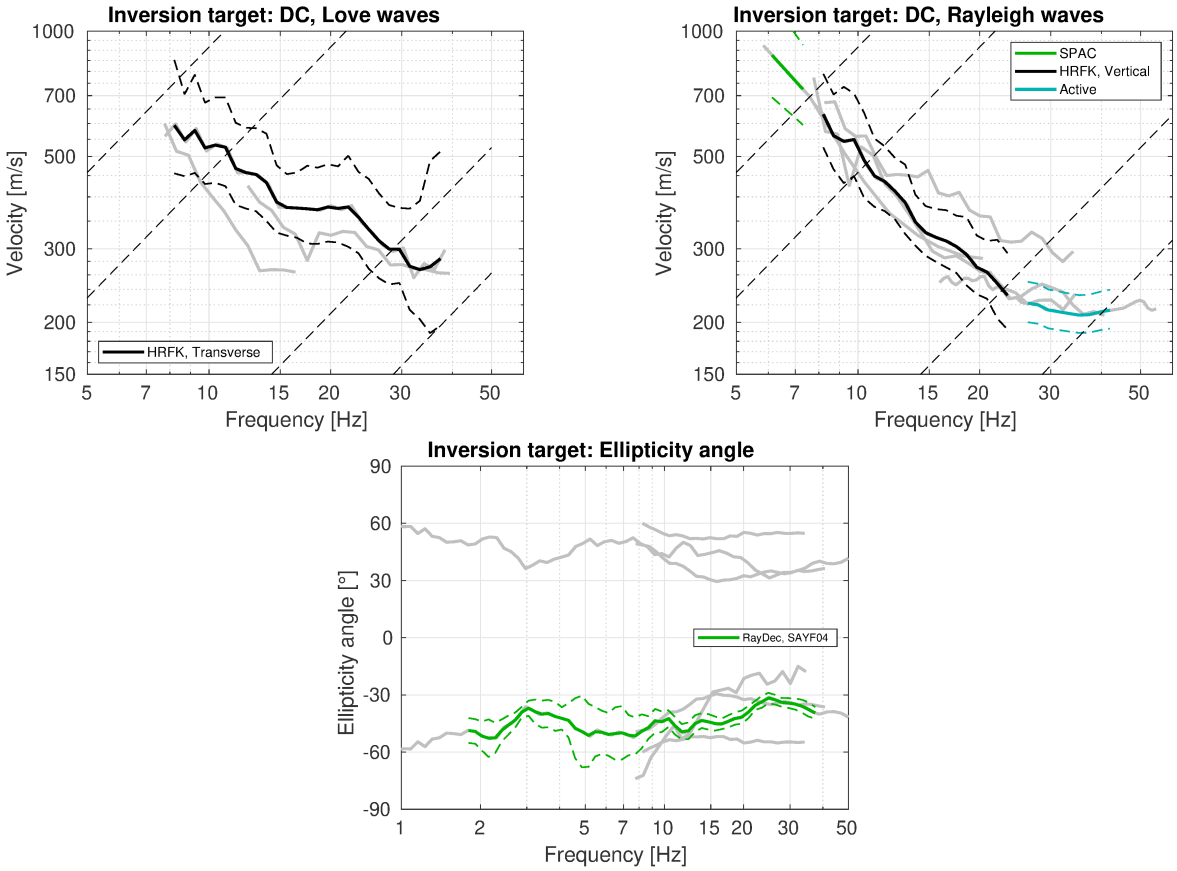


Figure 11: Overview of the dispersion (top) and ellipticity angle (bottom) curves used as targets for the different inversions.

Table 1: List of the different data curves used as target in the different inversions. For target 1, all listed curves where used. For target 2, the Love wave dispersion curve was not used.

| Method | Wave type | Mode | Curve type | Frequency range [Hz] |
|---|---|---|---|---|
| HRFK (T) | Love | fundamental | dispersion | 8.20 - 37.4 |
| SPAC | Rayleigh | fundamental | dispersion | 6.13 - 7.31 |
| HRFK (V) | Rayleigh | fundamental | dispersion | 8.20 - 23.5 |
| Active | Rayleigh | fundamental | dispersion | 26.3 - 42.0 |
| RayDec (SAYF04) | Rayleigh | fundamental | ellipticity angle | 1.80 - 37.4 |

## 4.3 Inversion results

We performed six inversions with different parameterizations. In Table 2, the obtained minimum misfit values for these inversions are shown. Each inversion run produced between 100 000 and 200 000 total models in order to assure a good convergence of the solution. For the 4-layer inversion, 100 000 generated models were sufficient, for the 5-layer inversion, 150 000. For all other parameterizations, around 200 000 models were generated. The results of the inversions SAYF4l to SAYFfix are shown in Figs 12 - 17
The different inversions for the respective targets yield similar misfit values and fit the data in a comparable way. The part of the Rayleigh wave dispersion curve coming from SPAC is not fitted, indicating that this part might either be badly estimated or correspond to a higher mode.

Table 2: List of inversions

| Inversion | Number of layers | Number of models | Minimum misfit |
|---|---|---|---|
| SAYF4l | 4 | 100 026 | 0.644 |
| SAYF5l | 5 | 150 011 | 0.630 |
| SAYF6l | 6 | 200 030 | 0.609 |
| SAYF7l | 7 | 199 997 | 0.609 |
| SAYF8l | 8 | 200 005 | 0.610 |
| SAYFfix | 20 | 200 048 | 0.617 |

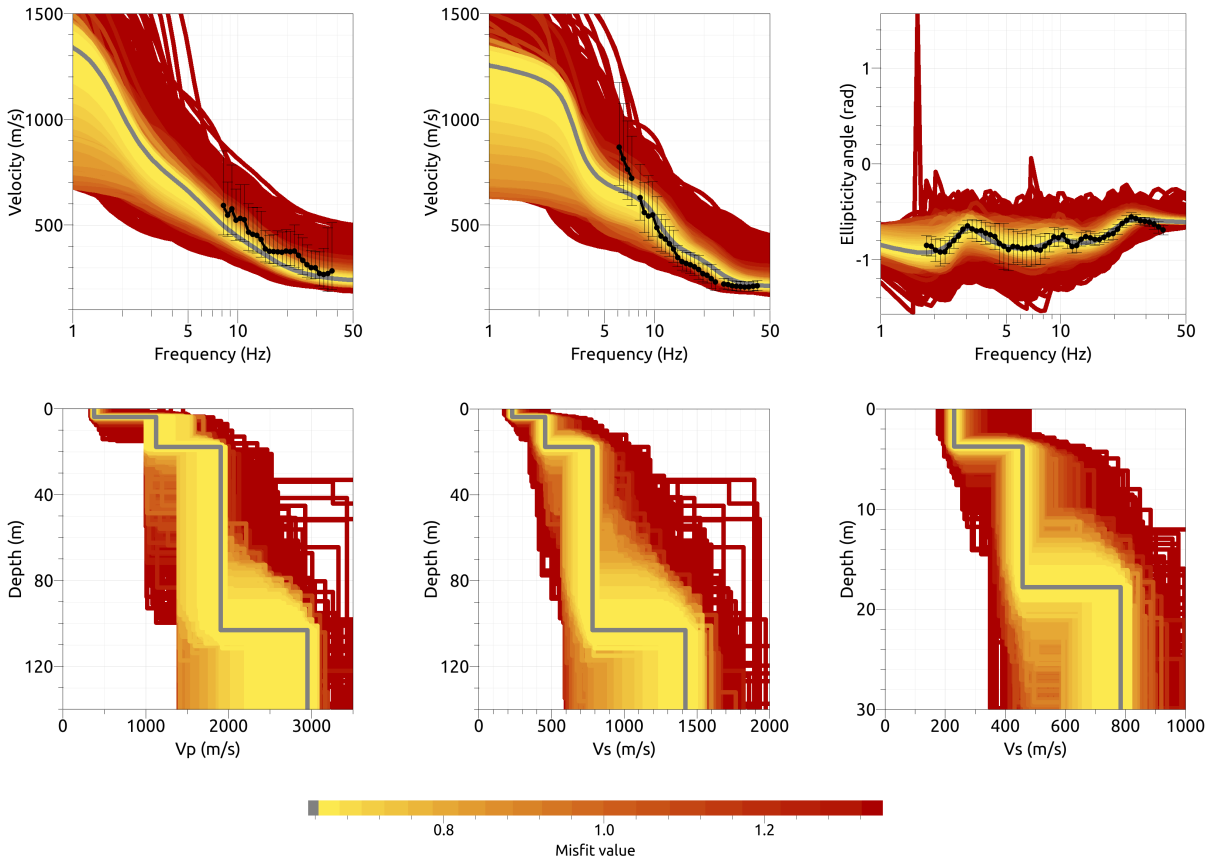


Figure 12: Inversion SAYF4l. Top line: Dispersion curves for Love waves (left) and Rayleigh waves (center) and Rayleigh wave ellipticity curves (right) of the respective fundamental modes. Bottom line: P-wave velocity profiles (left), S-wave velocity profiles (center and zoom on the right). The black dots indicate the data points used for the inversion, the gray line indicates the best-fitting model.

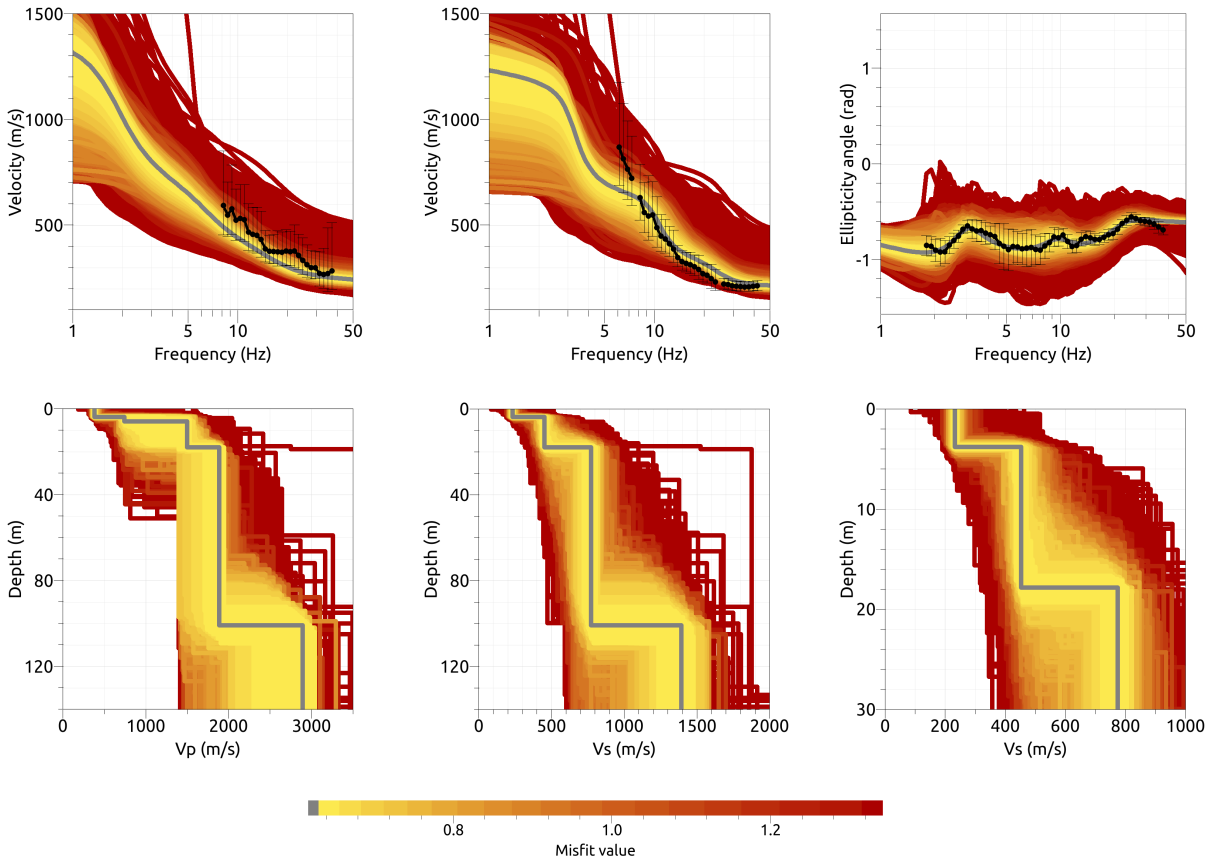


Figure 13: Inversion SAYF5l. Top line: Dispersion curves for Love waves (left) and Rayleigh waves (center) and Rayleigh wave ellipticity curves (right) of the respective fundamental modes. Bottom line: P-wave velocity profiles (left), S-wave velocity profiles (center and zoom on the right). The black dots indicate the data points used for the inversion, the gray line indicates the best-fitting model.

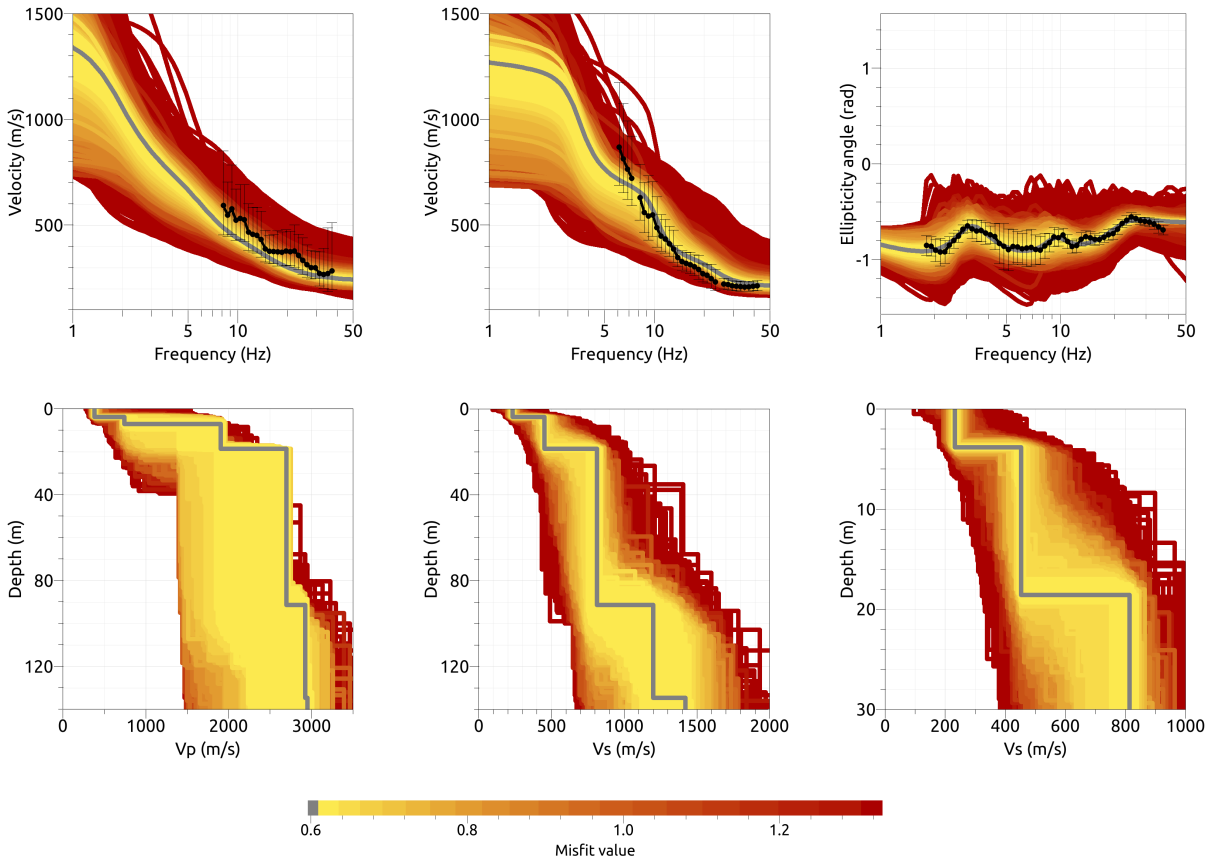


Figure 14: Inversion SAYF6l. Top line: Dispersion curves for Love waves (left) and Rayleigh waves (center) and Rayleigh wave ellipticity curves (right) of the respective fundamental modes. Bottom line: P-wave velocity profiles (left), S-wave velocity profiles (center and zoom on the right). The black dots indicate the data points used for the inversion, the gray line indicates the best-fitting model.

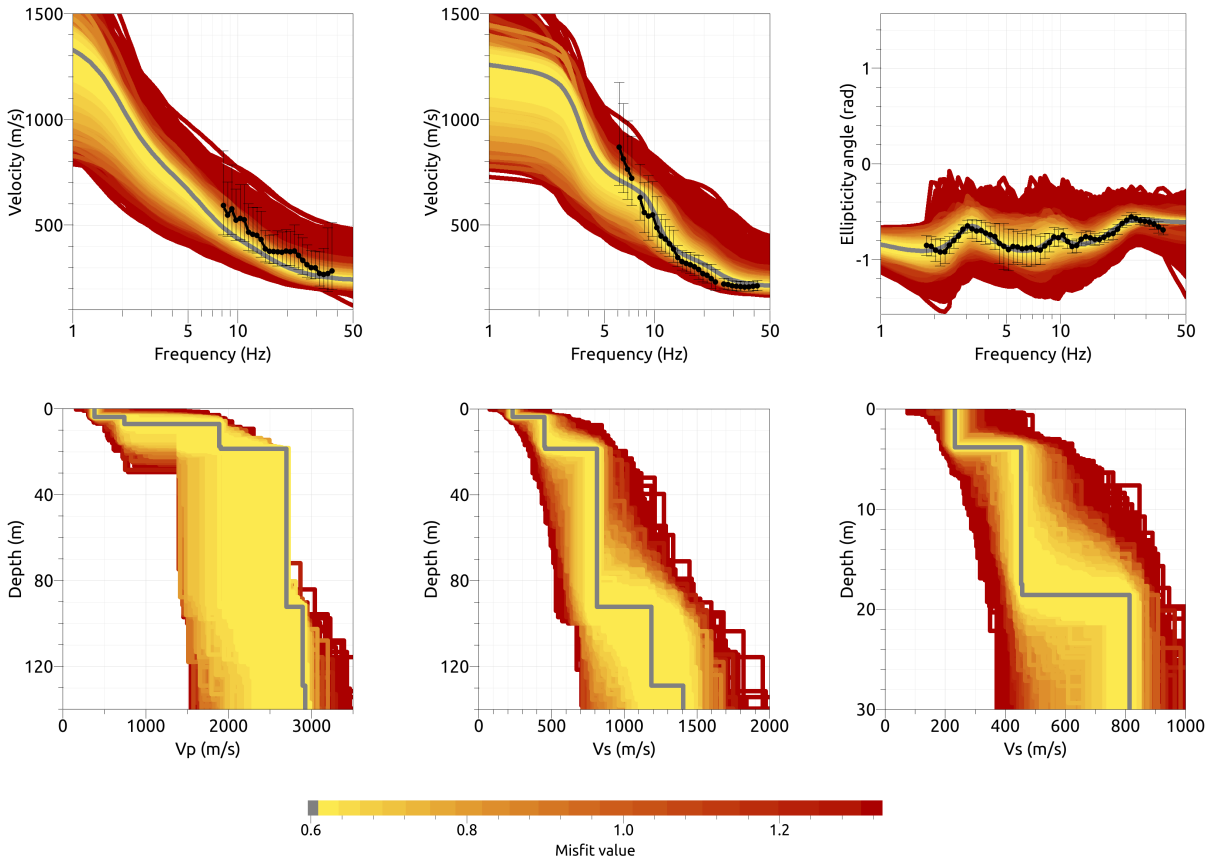


Figure 15: Inversion SAYF7l. Top line: Dispersion curves for Love waves (left) and Rayleigh waves (center) and Rayleigh wave ellipticity curves (right) of the respective fundamental modes. Bottom line: P-wave velocity profiles (left), S-wave velocity profiles (center and zoom on the right). The black dots indicate the data points used for the inversion, the gray line indicates the best-fitting model.

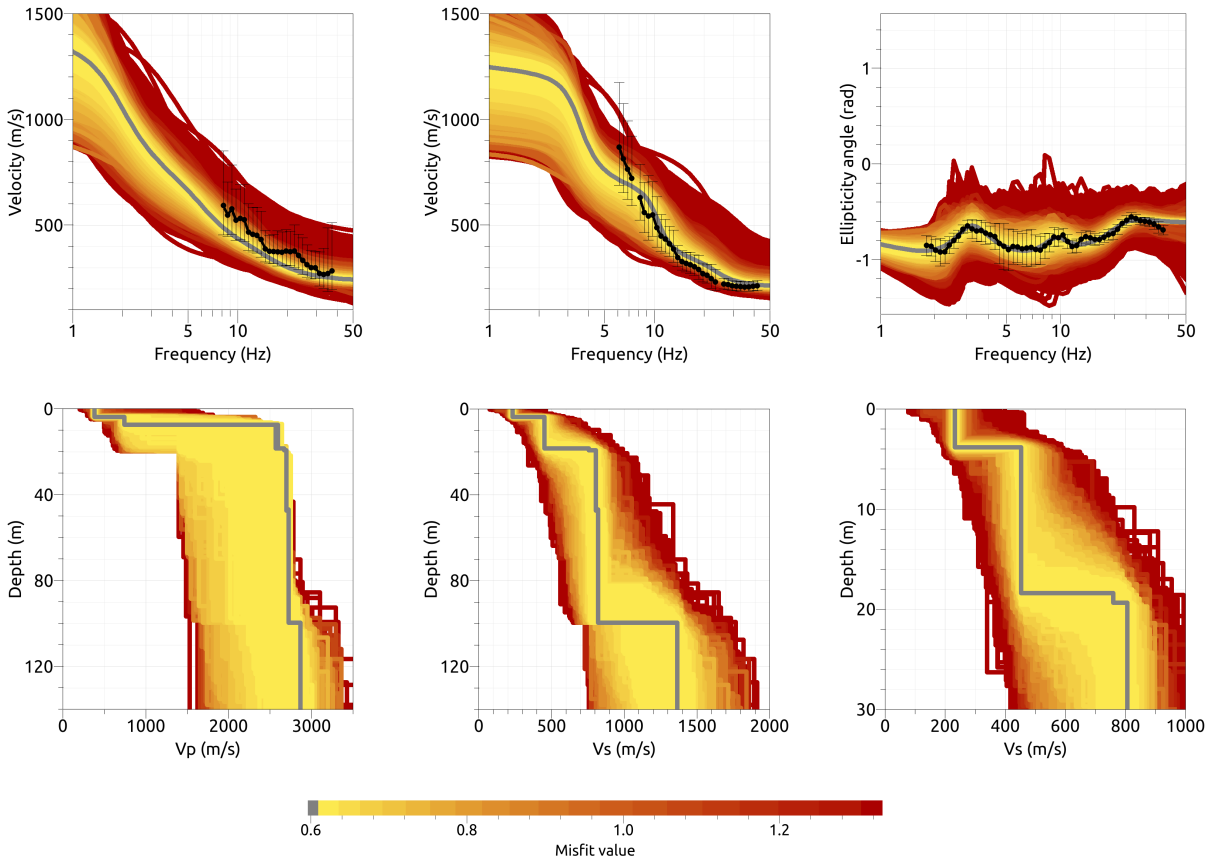


Figure 16: Inversion SAYF8l. Top line: Dispersion curves for Love waves (left) and Rayleigh waves (center) and Rayleigh wave ellipticity curves (right) of the respective fundamental modes. Bottom line: P-wave velocity profiles (left), S-wave velocity profiles (center and zoom on the right). The black dots indicate the data points used for the inversion, the gray line indicates the best-fitting model.

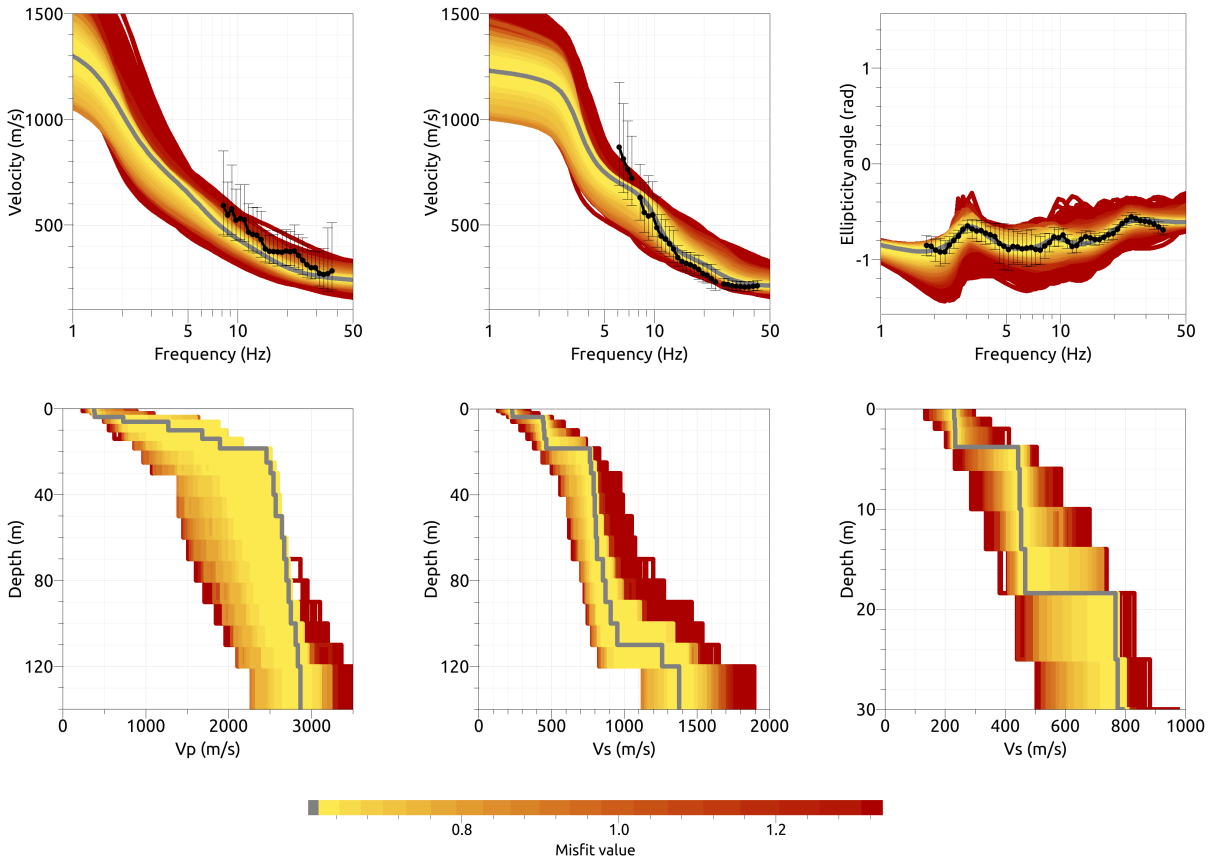


Figure 17: Inversion SAYFfix. Top line: Dispersion curves for Love waves (left) and Rayleigh waves (center) and Rayleigh wave ellipticity curves (right) of the respective fundamental modes. Bottom line: P-wave velocity profiles (left), S-wave velocity profiles (center and zoom on the right). The black dots indicate the data points used for the inversion, the gray line indicates the best-fitting model.

## 4.4 Overview of the inversion result

The S-wave velocity profiles of the best-fitting models of all inversions are shown in Fig. 18. The models of the respective targets show very similar main features and the larger flexibility of the models with more layers is hardly visible. A superficial layer with an S-wave velocity of around 230 m/s and thickness of 3.8 m is identified. Below, the velocity increases to around 455 m/s down to a depth of between 17.8 and 18.6 m. At this depth, the velocity increases to a value between 774 and 815 m/s. The next-deepest strong velocity contrast occurs between 90 m and 103 m of depth for the different models. The $V_{S30}$ values for the inversions range from 472.1 to 479.9 m/s (average value 476.2 $\pm$ 2.5 $m/s$). This corresponds to soil class B in EC8 and C in SIA261.
The depth at which the shear-wave velocity gets higher than 800 m/s varies between 18.6 m (these models actually correspond to soil class E in both EC8 and SIA261) and 103 m for the different models.

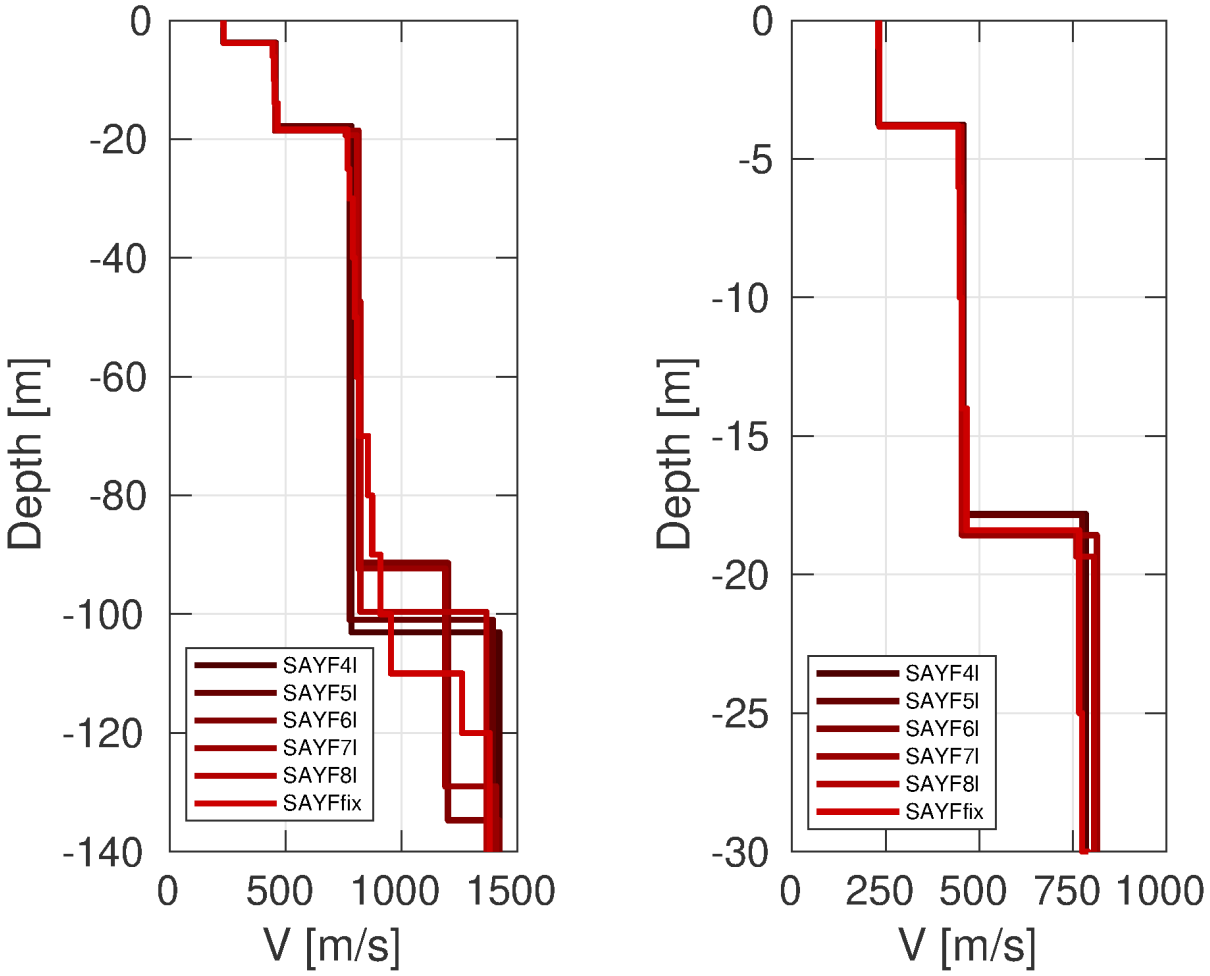


Figure 18: Overview of shear-wave velocity profiles of the best-fitting models of all inversions (left) and a zoom on the shallow part for the inversions using target 1 (center) and target 2 (right).

## 4.5 Amplification function

In Fig. 19, the theoretical amplification function for the best models resulting from the inversions is compared with the empirical amplification of station SAYF2, based on 116 events so far. The empirical amplification has values around 1 below 4 Hz and shows a first peak between 7 and 11 Hz, followed by a trough at 12.6 Hz and several small peaks above.
The modeled amplification for the models of the inversion shows an overall larger level of amplification with a first smooth peak around 2 Hz. Other peaks are found at 5.6 Hz and 8.0 Hz. A strong amplification peak occurs at 15.5 Hz. The different peak and trough frequencies are actually in rather good agreement with the empirical amplification, but the amplitudes differ.

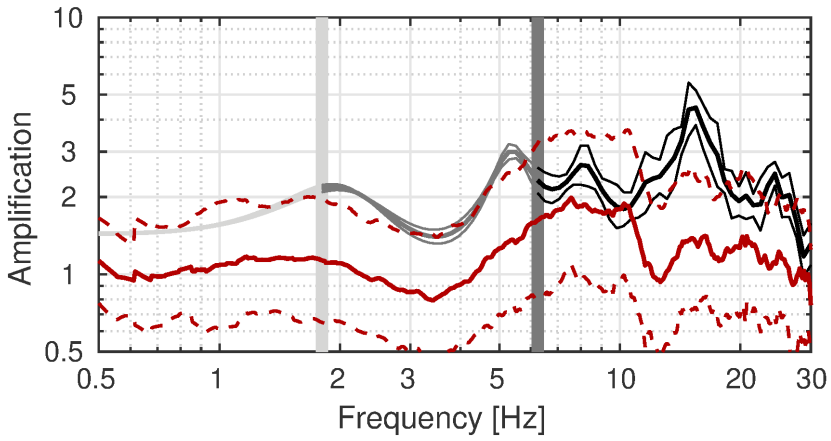


Figure 19: Comparison between the modeled amplification for the final set of best models of the different inversions (in grey to black, with standard deviation) and the empirical amplification measured at station SAYF2 (red, with standard deviation). The vertical light and dark grey bars correspond to the lowest frequency of the ellipticity and dispersion curves used for the inversion, respectively.

## 4.6 Quarter-wavelength representation

The quarter-wavelength velocity approach (Joyner et al., 1981) provides, for a given frequency, the average velocity at a depth corresponding to 1/4 of the wavelength of interest. It is useful to identify the frequency limits of the experimental data (the minimum frequency of the dispersion curve used in the inversion is 6.13 Hz, the minimum frequency used for the ellipticity inversion 1.80 Hz). The results using this proxy show that the dispersion curves constrain the profiles down to about 14.9 m and the ellipticity information down to about 94.8 m (Fig. 20). Moreover, the quarter wavelength impedance-contrast introduced by Poggi et al. (2012) is also displayed in the figure. It corresponds to the ratio between two quarter-wavelength average velocities, respectively from the top and the bottom part of the velocity profile, at a given frequency (Poggi et al., 2012). This curve shows several peaks at around 2 Hz, 5 Hz and 15 Hz.

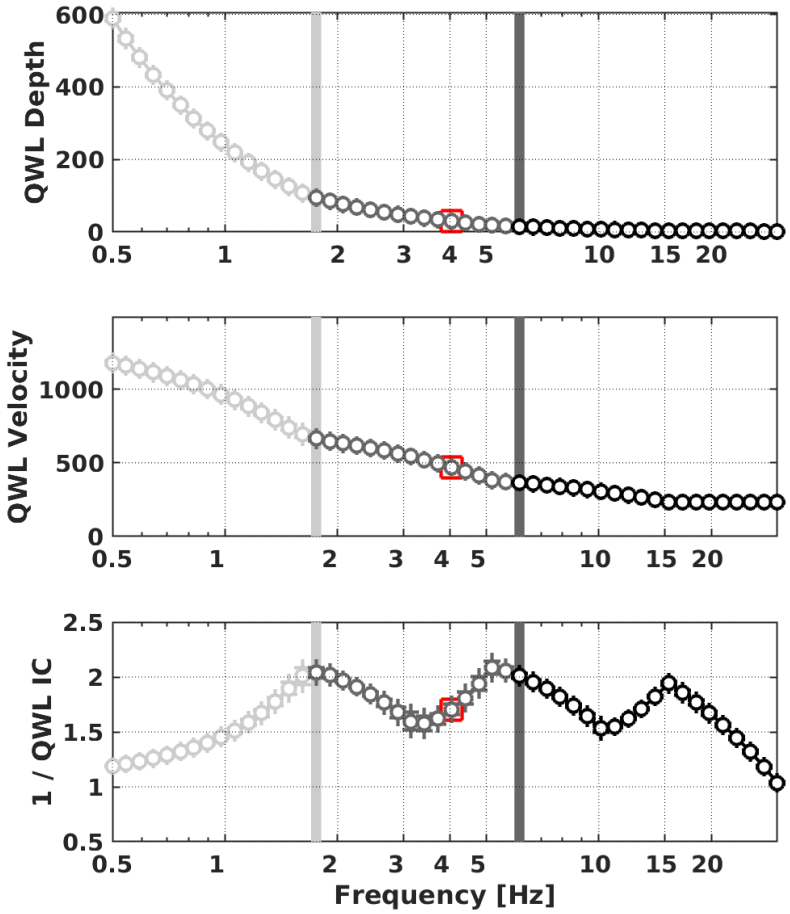


Figure 20: Quarter wavelength representation of the velocity profile for the best models of the inversions (top: depth, center: velocity, bottom: inverse of the impedance contrast) for the resulting models. The black curves are constrained by the dispersion curves, the light grey curves are not constrained by the data. The red square corresponds to $V_{S30}$.

# 5 Conclusion

We performed a passive array measurement and an active measurement to characterize the soil underneath station SAYF2 in Ayent-Fortunau (VS). According to the geological atlas, the station is located on fine-grained scree, but marl and moraine are close-by.
Using the passive experiment, the dispersion curves for Love and Rayleigh waves could be measured over a wide frequency range, from around 7.7 to 39.5 Hz for Love waves and from 5.8 to 40.7 Hz for Rayleigh waves. Using the active measurement, the Rayleigh wave dispersion curve can be identified between 15.9 and 64.7 Hz. In the H/V and ellipticity curves, a not very strong peak is found around 2.15 Hz and some stations show additional peaks between 5 and 10 Hz. The WaveDec result shows retrograde particle motion in the complete covered frequency range.
A joint inversion of the different measured curves, i.e. the Love and Rayleigh wave dispersion curves and the Rayleigh wave ellipticity angle, fits the data in a good way. The resulting models show a structure with a superficial layer of around 3.8 m thickness with a shear-wave velocity of around 230 m/s. The next layer has a velocity of about 455 m/s and reaches down to about 18 m, where the velocity increases to values of around 800 m/s. Another strong velocity contrast is found between 90 and 103 m. The $V_{S30}$ for the best models is about 476 m/s, corresponding to soil class B in EC8 and C in SIA261, but some models of the inversion actually correspond to class E in both EC8 and SIA261.

# Acknowledgements

The authors thank Oona Brunner and Dylan Longridge for their help during the array measurements.

# References


Aki, K. (1957). Space and time spectra of stationary stochastic waves, with special reference to microtremors. *Bull. Earthquake Res. Inst. Tokyo Univ.*, 35:415–456.

Bettig, B., Bard, P.-Y., Scherbaum, F., Riepl, J., Cotton, F., Cornou, C., and Hatzfeld, D. (2001). Analysis of dense array noise measurements using the modified spatial auto-correlation method (SPAC): application to the Grenoble area. *Boll. Geof. Teor. Appl.*, 42:281–304.

Burjánek, J., Gassner-Stamm, G., Poggi, V., Moore, J. R., and Fäh, D. (2010). Ambient vibration analysis of an unstable mountain slope. *Geophys. J. Int.*, 180:820–828.

Burjánek, J., Moore, J. R., Molina, F. X. Y., and Fäh, D. (2012). Instrumental evidence of normal mode rock slope vibration. *Geophys. J. Int.*, 188:559–569.

Fäh, D., Wathelet, M., Kristekova, M., Havenith, H., Endrun, B., Stamm, G., Poggi, V., Burjanek, J., and Cornou, C. (2009). Using ellipticity information for site characterisation. NERIES deliverable JRA4 D4, available at http://www.neries-eu.org.

Hobiger, M., Bard, P.-Y., Cornou, C., and Le Bihan, N. (2009). Single station determination of Rayleigh wave ellipticity by using the random decrement technique (RayDec). *Geophys. Res. Lett.*, 36.

Joyner, W. B., Warrick, R. E., and Fumal, T. E. (1981). The effect of Quaternary alluvium on strong ground motion in the Coyote Lake, California, earthquake of 1979. *Bull. Seismol. Soc. Am.*, 71(4):1333–1349.

Maranò, S., Reller, C., Loeliger, H.-A., and Fäh, D. (2012). Seismic waves estimation and wavefield decomposition: Application to ambient vibrations. *Geophys. J. Int.*, 191:175–188.

Poggi, V., Edwards, B., and Fäh, D. (2012). Characterizing the Vertical-to-Horizontal ratio of ground motion at soft-sediment sites. *Bull. Seismol. Soc. Am.*, 102(6):2741–2756.

Poggi, V. and Fäh, D. (2010). Estimating Rayleigh wave particle motion from three-component array analysis of ambient vibrations. *Geophys. J. Int.*, 180:251–267.

Wathelet, M., Jongmans, D., and Ohrnberger, M. (2005). Direct inversion of spatial autocorrelation curves with the neighborhood algorithm. *Bull. Seismol. Soc. Am.*, 95:1787–1800.